Solid Propellant Combustion Zone Structure from Analysis of Hydroxyl Radical Chemiluminescence

D.H. Campbell* and S. Hulsizer*
University of Dayton Research Institute, Air Force Rocket Propulsion Laboratory
Edwards Air Force Base, California
and
T. Edwards† and D.P. Weaver†
Air Force Rocket Propulsion Laboratory, Edwards Air Force Base, California

Hydroxyl radical chemiluminescence spectra have been obtained in the combustion zone above ammonium perchlorate composite solid propellant burning at multiatmospheric pressures in a laboratory scale strand burner. These semiresolved (.13 nm) spectra were analyzed by constructing OH synthetic spectra and employing a best-fit technique to determine the rotational temperature and vibrational population distribution in the $A^2\Sigma^+$ electronic state of OH in the flame. Values for rotational temperature and vibrational population distribution were obtained for pressures from 0.2 to 7.0 MPa at three positions above the propellant surface. Quantitative comparison of results over a range of pressures for a given spatial position is mitigated by the potentially significant effects of self absorption on the measured spectra. Comparisons at a given pressure for various positions above the propellant surface should not be affected by self-absorption, and show a fairly constant rotational temperature and vibrational population distribution from near the surface out to the maximum position investigated (12 mm). These results indicate that a chemical combustion environment involving short lived radical species exists at distances very far from the propellant surface even at elevated pressures. Interpretation of the spectral characteristics of the emission data also indicates highly nonequilibrium vibrational populations and possible non-Boltzmann rotational distributions which increasingly diverge from equilibrated distributions with increasing pressure.

Nomenclature

I_{exp} = experimental spectral peak intensity
I_{calc} = calculated synthetic spectral peak intensity
N_0 = number density in $v' = 0$
N_1 = number density in $v' = 1$
T_R = rotational state temperature
v' = excited electronic state vibrational quantum number
v'' = ground electronic state vibrational quantum number

I. Introduction

AN important goal of all solid propellant programs is the ability to tailor propellant ballistic properties and performance through the selective modification of propellant ingredients. At present, the desired propellant properties are obtained by alteration of ingredient chemical and physical properties based on a mixture of experience and trial-and-error experimentation. A more fundamental approach would use computer models to predict the chemical and physical processes that occur during solid propellant combustion. Unfortunately, present propellant combustion models[1-3] consolidate the specific details of propellant chemistry into a global or overall kinetic equation, and are therefore unable to explain the significant change in macroscopic propellant properties (such as burning rate) that can occur from apparently minor changes in formulation (such as a change in curative agent).[4] Future propellant combustion models will need to include more detailed chemical kinetic processes to be able to predict these effects. Identification of the important chemical processes occurring in the combustion zones above the surface of burning propellant is thus a vital step toward an ability to predict propellant burning characteristics using combustion models.

As a first step toward a more detailed understanding of solid propellant combustion processes, a survey of the naturally occurring emission from ammonium perchlorate (AP/HTPB) and nitramine (HMX) propellants at elevated pressures has been made for the wavelength range 280.0-800.0 nm. A detailed discussion of these results and a more complete discussion of the history and background of propellant flame emission measurements are given in Ref. 5. This paper contains the results of any analysis of the emission spectra from AP/HTPB propellant flames in the region of hydroxyl radical (OH) chemiluminescence. A technique is described and used for the determination of OH $A^2\Sigma^+$ state rotational temperature and vibrational population distribution from the semiresolved (.13 nm resolution) OH emission spectra. Because of the short radiative lifetime (.66 μs) of the hydroxyl radical compared to flow times, OH emission marks the spatial position at which the excited state OH is produced. Production of OH in the $A^2\Sigma^+$ state in these flames is strictly through direct exothermic chemical reactions.[6] The thermal population of the $A^2\Sigma^+$ state at 3000 K is about 10^{-7} that in the ground $X^2\Pi$ state, so that no significant thermally produced excited state population will exist in the flame. The internal energy state populations will be indicative of the local chemical combustion process, altered by some (possibly large) amount of collisional redistribution of population.

The spectral emission measurements described here and in Ref. 5 are being used to examine the overall flame structure of burning solid propellants, and to direct more detailed experimental studies using laser-induced fluorescence and laser Raman diagnostic techniques.[7]

Received June 18, 1985; revision received Feb. 19, 1986.

*Research Physical Scientist.
†Research Physical Scientist. Member AIAA.

II. Experimental Approach

To simulate correctly the chemical combustion processes of solid propellants, measurements must be made at conditions within a range characteristic of the temperature, pressure, and high heating rates encountered in the solid propellant rocket engine. This is accomplished by burning 6-mm-diam strands of propellant in a high-pressure combustion chamber equipped with 3-cm-diam sapphire windows for optical access.[8,9] A servopositioning system using an He-Ne laser beam referencing system keeps the burning surface of the propellant at a constant height relative to the optical-detection system. A high-pressure nitrogen flow from the base of the propellant holder purges the chamber of combustion products and helps prevent deposition on the windows. The system is capable of operating up to about 7.0 MPa (1000 psi). The AP/HTPB propellant samples are water-washed and coated with a fluorocarbon grease to inhibit side burning. Burn times range from 1-10 s depending on the chamber pressure. The servocontrol electronic system contains a circuit which counts step pulses and elapsed time, and which can be used to give directly the burn rate of the propellant sample.

The optical collection system and detection equipment setup are shown schematically in Fig. 1. The optical system turns the image of the propellant flame 90 deg so that the vertical entrance slit of the spectrometer defines a horizontal sampling volume 500-1000 μm wide, depending on the slit width necessary to obtain sufficient signal-to-noise ratios. The collected light is dispersed by an SPEX Triple-Mate Spectrometer and detected by an EG&G/PAR Reticon diode array detector. All of the 500 pixel spectra are stored on floppy disks and can also be output to a plotter for qualitative analysis. Detector software allows multiple spectra to be recorded during each burn. Each read scan of the detector surface takes approximately 11 ms. The charge on the detector is allowed to build up for a given number of scan times before it is read, so that each of the recorded spectra is a snapshot of the emission from the burning propellant with a time resolution depending on the number of buildup intervals (usually 5-10). Typical photon count rates per channel for each spectra were in the 500-1000 range. Dark counts were typically 300-500 per channel and were determined before a run was made, stored, and subtracted from the flame emission spectra data before any hard copy output or analysis were performed.

The diagnostic position above the propellant surface is defined by the position of a laser beam aligned with the detector optical system. The He-Ne surface referencing beam is moved with respect to this position beam to move the collection volumn relative to the propellant surface. The spatial distance between the two beams is found by steering the propellant from the surface positioning beam to the optical position beam and recording the number of servosteps between the two positions. For AP propellants burning at pressures above 3.5 MPa, the servo-control mechanism was unable to hold the propellant surface at a constant position due to intermittent blocking of the surface referencing laser beam by heavy concentrations of particulate matter. Consequently, the position was accurate to only about 0.6 mm for the 3.5 MPa condition, and about 1.1 mm for the 7.0 MPa condition. The position accuracy was about 0.1 mm for pressures below 3.5 MPa.

For the analysis of OH spectra, it was necessary to calibrate the frequency response of the optical-detection system in the 308.0-316.0 nm range. This was accomplished by placing a quartz-halogen standard lamp outside the chamber window opposite the window through which the emission radiation is collected. The spectrometer slits and filter stage grating positions were set to the same values as used during OH emission data collection. In this way, a frequency response and a pixel sensitivity calibration are acquired simultaneously. The only difference between the calibration and the data acquisition setup is that the calibration lamp radiation passes through two combustion chamber windows instead of one. The windows are made of identical sapphire material, and it is assumed that they will have the same frequency-dependent absoption characteristics, if not the same absolute total absorption factor.

III. Analysis Technique

The OH emission spectra obtained for various positions above the propellant surface contain sufficient information about the internal energy states of the $A^2\Sigma^+$ electronic state of OH (from which the emission originates) to allow a determination of the populations in these rotational and vibrational levels. The spectra between 306.0 and 316.0 nm contain most of the 0-0 vibrational band of the $A^2\Sigma^+ \rightarrow X^2\Pi$ electronic transition of OH, as well as a large portion of the 1-1 band. The position of the major lines in these two band systems is shown in Fig. 2. All of the major lines in the 1-1 band lie at wavelengths greater than 312.1 nm, whereas most of the 0-0 band lies at wavelengths less than 312.1 nm. This separation allows determination of the relative population in the $v'=0$ and $v'=1$ vibrational states.

To determine the internal energy state population distributions from the experimental spectra (Fig. 3), a "synthetic" spectra is constructed using the known OH molecular parameters and the spectrometer-detector characteristics. At the resolution of the detection system in this experiment, each spectral peak in the OH spectra is typically the result of transitions from a number of rotational-vibrational levels; therefore, Boltzmann plots[10,11] and/or isointensity plots,[12] which have been used previously to acquire rotational temperatures from resolved OH flame emission spectra, cannot be used in this case. Additionally, since the OH spectral lines are not completely resolved, there is no way to decon-

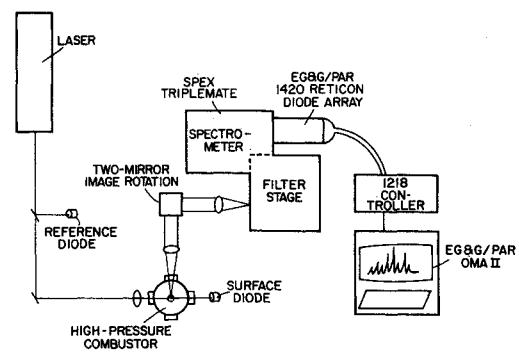

Fig. 1 Experimental optical-detection system for acquisition of propellant emission spectral data.

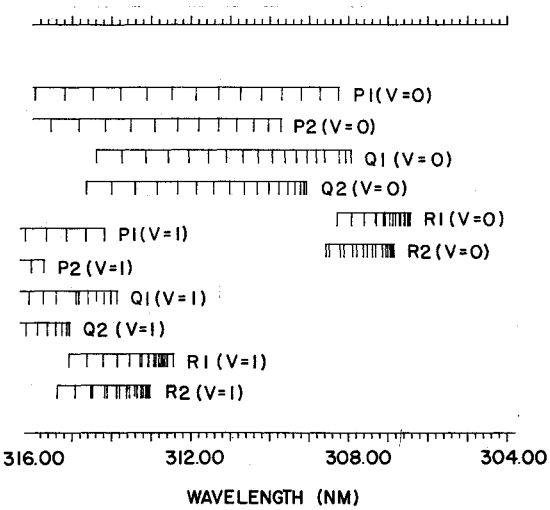

Fig. 2 Positions of the major lines for the 0-0 and 1-1 bands of the A-X OH transition.

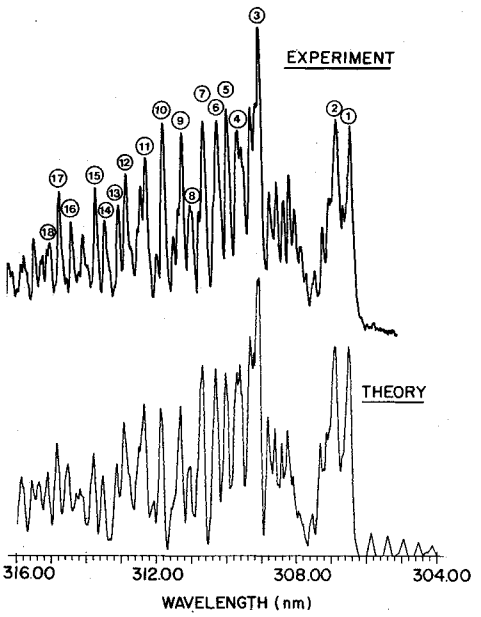

Fig. 3 Comparison of experimental OH spectra and synthetic spectra calculated using $T_R = 2350$ K and $N_1/N_0 = 0.66$.

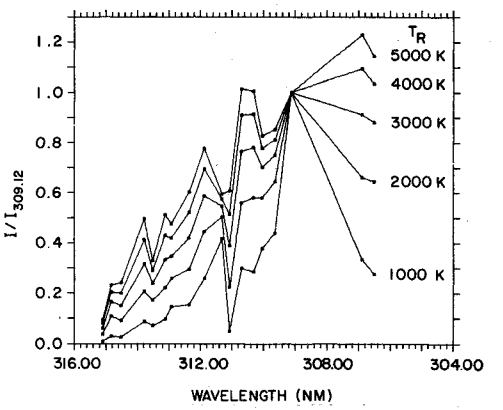

Fig. 4 Variation of the relative peak heights in the OH spectra with rotational temperature for $N_1/N_2 = 0$. All peaks increase in relative intensity with increasing temperature.

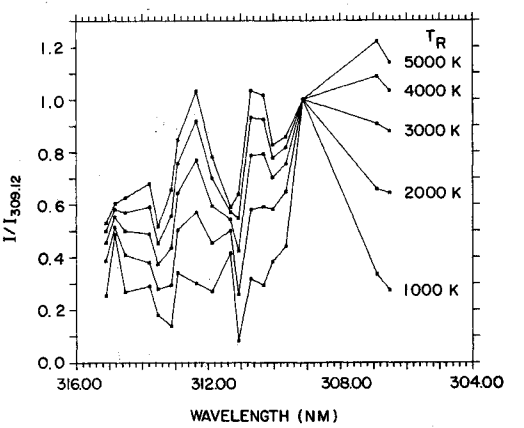

Fig. 5 Variation of the relative peak heights in the OH spectra with rotational temperature for $N_1/N_2 = 1$. All peaks increase in relative intensity with increasing temperature.

volve the spectral intensities into an arbitrary distribution of population in the rotational states. Consequently, it is necessary to assume that the rotational population will follow a Boltzmann distribution given by some specific "temperature." This temperature should not be confused with the actual gas kinetic temperature, as it only indicates the rotational temperature in the OH $A^2\Sigma^+$ electronic state, which may or may not be the same as the gas kinetic temperature.

Eighteen peaks are chosen from the experimental spectra (Fig. 3) for determination of the rotational and vibrational state distributions. All of the measured experimental and synthetically calculated intensities are normalized by the intensity at 309.12 nm (vacuum wavelength), which is typically the highest peak and is the location of the Q_2 (0-0) band head. As such, its intensity will be dominantly dependent on the population in the lowest four-rotational levels of the $v' = 0$ state. Most of the other peaks in the area of the 0-0 band have significant contributions from higher rotational levels, and therefore will vary in intensity relative to the Q_2 head with changes in temperature.

The synthetic spectra are calculated using the term values from Coxon[13] and the relative Einstein A coefficients calculated by Chidsey and Crosley.[14] All of the main (P_1,P_2,Q_1,Q_2,R_1,R_2) and satellite rotational band sequences (Q_{12},P_{12},R_{21},Q_{21}) are used in constructing the spectra. The spectrometer slit function is assumed to be triangular, and the bandpass is adjusted to give a spectrum similar in shape to the experimental spectra (0.13 nm). Experimental and synthetically generated spectra are shown in Fig. 3 to illustrate qualitatively the similarity in the two spectra after the rotational and vibrational populations have been determined. Also shown are the positions of the 18 peaks used in determining the internal state populations.

The sensitivity of the relative peak heights to rotational temperature is shown in Figs. 4 and 5 for two different vibrational distributions. In these synthetic spectra calculations, it is assumed that both $v' = 0$ and $v' = 1$ rotational populations follow Boltzmann distributions at the same given temperature. The results indicate that sufficient sensitivity to rotational temperature exists to determine an accurate value of this parameter. In fact, sufficient sensitivity exists in the relative intensities of peaks 1 or 2 to peak 3 to produce an accurate value of the rotational temperature simply by using one of these relative intensities. This is the technique used by Vaidya et al.[15] to acquire flame temperatures in the region outside the primary reaction zone of methane-air flames with various amounts of added coal. In our case, a multiple peak fit is used to detect any deviation from equilibrium population distributions.

The sensitivity of relative peak heights to vibrational population is shown in Fig. 6 for a representative rotational temperature. Again, the contribution of $v' = 1$ rotational populations to the spectra is confined primarily to wavelengths above 312.1 nm, with the variation in the peak heights in this region being sufficient to produce an accurate measure of the relative population in $v' = 0$ and $v' = 1$. Note that a rise in either rotational temperature or $v' = 1$ population will increase the intensities of peaks 11-18.

Due to the variation of peaks 11-18 with both T_R and vibrational population, the fitting procedure to match synthetic spectra for determination of rotational and vibrational distribution first uses peaks 1-10 to determine a rotational temperature by finding the least-squares best fit of the experimental peaks to the calculated peaks. The computer code iterates on temperature with a given temperature step size (20 K in all of the results given here), and uses a vibrational population ratio of 1.0, until the ten calculated points form the best fit to the experimental points. Once T_R is found, peaks 11-18 are used to find the best fit to the relative population in $v' = 0$ and $v' = 1$ (vibrational ratio step size is 0.02). Using these results (T_R,N_1/N_0), the 18 synthetic spectra peaks are recalculated and the whole process is repeated if any of the intensities of peaks 1-10 deviate substantially from the results of the first calculation due to a significantly different vibra-

tional population than was assumed originally for the rotational temperature fitting procedure (peaks 7 and 8 have a slight vibrational population dependence; see Fig. 6).

The above analysis assumes $T_R(v'=0) = T_R(v'=1)$, which may not be the case if the combustion processes which produce excited electronic state OH are such that highly nonequilibrium internal energy state distributions are produced. The calculation is therefore repeated, using the best fit T_R for $v'=0$ and letting T_R $(v'=1)$ vary. Iteration on T_R $(v'=1)$ and N_1/N_0 using peaks 11-18 then completes the calculation. Unfortunately, each $v'=1$ point increases with both v'total population and $v'=1$ rotational temperature, so that a unique solution for T_R $(v'=1)$ and N_1/N_0 is not possible. The relative magnitude of the change in each peak does differ for changing vibrational population compared to the change for rotational temperature variation. Consequently, it is possible calculate a least-squares best fit to these two parameters. The result may not be a real reflection of the vibrational and rotational populations in $v'=1$ due to random experimental error in the data, but it may give some indication of the possible difference in the rotational temperatures in the two vibrational levels.

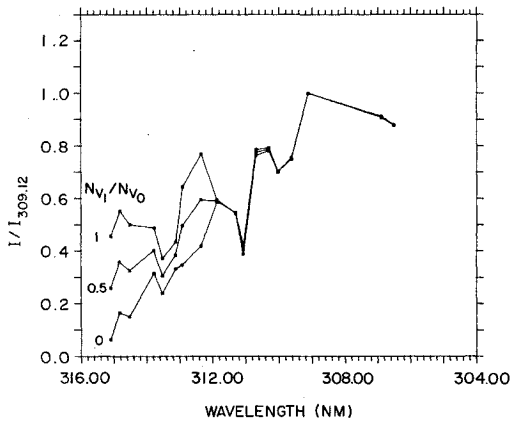

Fig. 6 Variation of the relative peak heights in the OH spectra with vibrational population distribution for $T_R = 3000$ K.

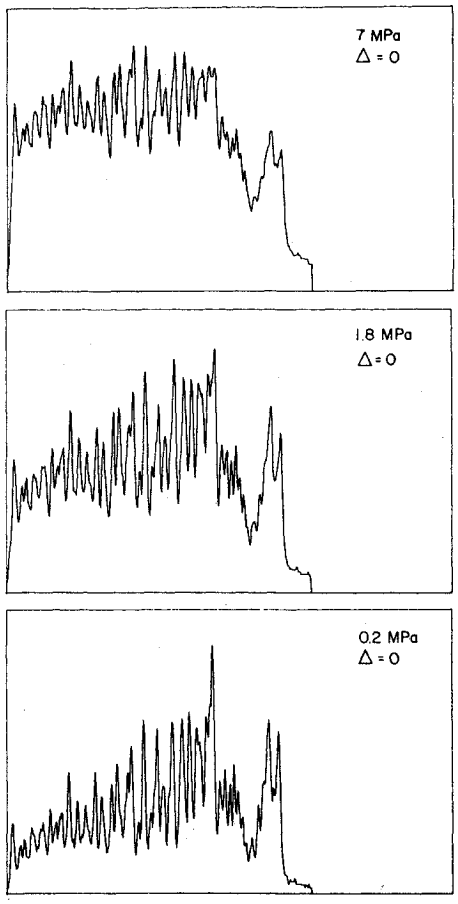

Fig. 7 OH emission spectra variation with pressure.

IV. Results and Analysis

A sequence of emission spectra from AP/HTPB propellant for the wavelength interval between 306 and 316 nm is shown in Fig. 7 for a series of pressures at a position centered on the propellant surface. The increase in intensity of the high-wavelength side of the spectra relative to the first two peaks on the low-wavelength side with increasing pressure is not due entirely to increased $v'=1$ population relative to $v'=0$ or to increased rotational temperature. A continuum emission underlies the OH spectra and increases in intensity with increasing pressure. This continuum is shown clearly in Fig. 8, which shows a spectrum, obtained using a grating with one

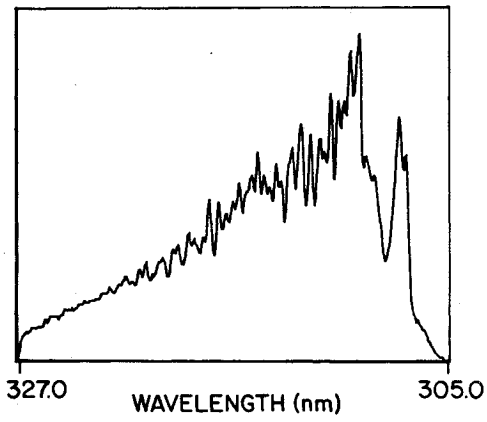

Fig. 8 Extended wavelength range experimental OH emission spectra.

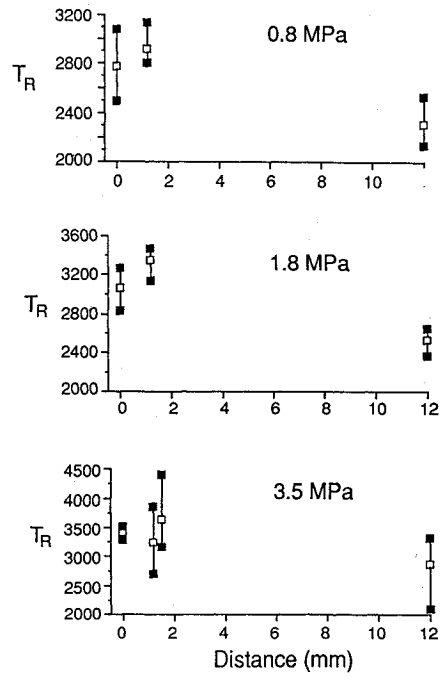

Fig. 9 Rotational temperature ($v'=0$) variation with pressure and distance above surface. Open squares are average values, filled squares are average values, filled squares are high and low values for multiple spectra taken during each burn.

Table 1 Best fit rotational temperature

Position above surface, μm	Pressure, MPa	Number of traces	$v'=0$ Average rotational temperature, K	$v'=0$ Standard deviation σ, K	$v'=1$ Average rotational temperature, K	$v'=1$ Standard deviation σ, K
0	0.2	4	2330	92.2	1645	427.4
0	0.8	5	2776	190.7	1372	150.0
0	1.8	5	3064	188.2	1540	120.0
0	3.5	5	3444	90.7	1500	142.5
0	7.0	5	3665	109.9	2032	548.0
1200	0.8	4	2915	130.7	1365	207.1
1200	1.8	5	3344	131.9	1444	128.0
1200	3.5	5	3244	410.8	1645	550.3
1200	3.5	5	3656	457.4	1436	206.1
1200	7.0	4	3675	283.3	1525	238.5
1200	0.8	5	2320	141.8	1708	476.4
1200	1.8	6	2537	95.0	2537	95.0
1200	3.5	4	2870	488.0	2870	488.8

half the dispersion of the one used to obtain the spectra shown in Fig. 7. This continuum is subtracted from the measured peak heights before the rotational temperature and vibrational populations are determined. The technique used to obtain background continuum-corrected intensities is explained in detail in Appendix A.

Using the 18-peak fitting technique, the relative population in vibrational levels $v'=0$ and $v'=1$ and the rotational temperatures in these vibrational levels were determined for a series of pressures and positions above the propellant surface. The results of the fitting calculations are shown in Tables 1 and 2 and Fig. 9. Between 4 and 6 spectra were recorded during each burn. The average rotational temperatures and vibrational distribution for each burn are shown in the table, with the standard deviation of the individual results for each spectrum taken during each burn. The spatial distribution of the rotational temperature in $v'=0$ for three pressure conditions are shown in the figures, where the error bars show the high and low rotational temperature for the multiple spectra taken during each burn.

Some general trends in the results are apparent. The average rotational temperature for $v'=0$ increases quite smoothly with increasing pressure at each spatial position. In addition, for a constant pressure, the $v'=0$ rotational temperature is maximum at the intermediate position. The standard deviation is small enough in most cases to verify that these trends are real. One condition where the standard deviation is relatively large is at 3.5 MPa at the middle spatial position (1.2 mm). This condition was run twice, and both burns produced a sequence of spectra which yielded widely varying $v'=0$ rotational temperatures. The variation in rotational temperature during each burn may not be due purely to random experimental error. It is possible that the variation is real and reflects a fluctuating combustion environment. The large variation in T_R during burns at some specific conditions may mean that the combustion process produces large temporal fluctuations at those conditions compared to other, more quiescent conditions.

The results for $v'=1$ rotational temperature and vibrational population ratio are somewhat more random in value and have more cases with large standard deviations than do the $v'=0$ rotational temperature results. There is a slight trend toward higher N_1/N_0 vibrational population ratios as the pressure increases at each position. Also, it is of note that when a separate $v'=1$ temperature is calculated, the best-fit vibrational population and $v'=1$ temperatures decrease from the values calculated assuming $T_R(v'=0)=T_R(v'=1)$. This is somewhat unexpected, since the values of peaks 11-18 used to fit the $v'=1$ region all are decreased with reductions in either $T_R(v'=1)$ or N_1/N_0. The improved fit (up to 5 times better in some cases) over that for equivalent rotational temperatures is due to the change in relative magnitudes of peaks 11-18; this change overcomes the effect of the overall lowering of the peaks with reduced values of the fit variables. A detailed analysis of the results for each trace in a burn shows that the iterative best-fit routine can sometimes produce significantly different values for $T_R(v'=1)$ and N_1/N_0 with only a small difference in the total sum of the squared deviation ($\Sigma[I_{\text{exp}}-I_{\text{calc}}]^2$). This is not necessarily an indication that the fit routine is improperly evaluating the results, but rather it results from the nonunique combinations of $T_R(v'=1)$ and N_1/N_0 that produce the best fit to the experimental data for peaks 11-18. Consequently, the results for $T_R(v'=1)$ and N_1/N_0 must be viewed with some measure of caution, especially in light of the additional errors introduced by self-absorption effects (see next section).

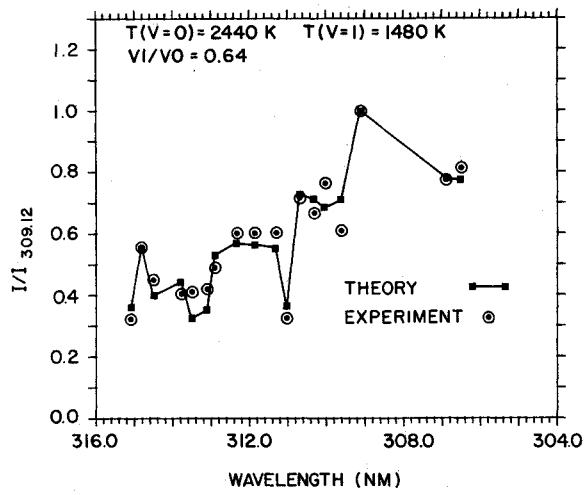

Fig. 10 Best-fit results for position = 0 μm, pressure = 0.2 MPa.

The fit of the experimental data to the calculated theoretical spectra is shown in Figs. 10-12 for three pressures at a position centered on the surface of the propellant. The fit for both $v'=0$ rotational temperature (10 low wavelength points in the figures) and $v'=1$ temperature and population (8 high wavelength points) is fairly good for the lowest pressure, but worsens as pressure increases. The divergence is especially noticeable in the 10th point in the $v'=0$ region. This suggests that the population distribution in the rotational levels of the OH excited state does not follow a Boltzmann distribution at the best-fit temperature, and that the degree of nonequilibrium may increase with increasing pressure.

Table 2 Best fit vibrational population ratio

Position above surface, μm	Pressure, MPa	$T_0 = T_1$ Average N_1/N_0	$T_0 = T_1$ Standard deviation σ	$T_0 \neq T_1$ Average N_1/N_0	$T_0 \neq T_1$ Standard deviation σ
0	0.2	0.62	0.095	0.71	0.090
0	0.8	0.76	0.051	1.04	0.046
0	1.8	0.80	0.015	1.11	0.065
0	3.5	0.90	0.037	1.32	0.020
0	7.0	0.98	0.160	1.36	0.205
1200	0.8	0.60	0.038	0.85	0.010
1200	1.8	0.68	0.032	1.04	0.064
1200	3.5	0.80	0.280	0.94	0.156
1200	3.5	0.71	0.097	1.08	0.114
1200	7.0	0.75	0.185	1.15	0.253
12000	0.8	0.74	0.115	0.86	0.155
12000	1.8	0.66	0.097	0.78	0.080
12000	3.5	0.97	0.118	1.10	0.161

Table 3 Self-absorption model best fit results ($T_R = 2000$ K, $N_1/N_0 = 0.25$)

P, MPa	$T_R(v'=0)$	$T_R(v'=1)$	N_1/N_2
0.2	2120	1840	0.29
0.8	2580	1640	0.37
1.8	3260	1520	0.51
3.5	4020	1440	0.74
7.0	4820	1660	1.23

Table 4 Concentration and rotational temperature gradient effects on self-absorption

T_R, K	Pressure, MPa	$T_R(v'=0)$	$T_R(v'=1)$
2000	3.5	4020	1440
2000	Peak	4040	1560
2000	Valley	4020	1560
Peak	3.5	3820	1420
Valley	3.5	3840	1320

The generally high level of vibrational excitation at all conditions is of particular note. The population in $v'=1$ for an equilibrium Boltzmann distribution at 3000 K is about 20% of the population in $v'=0$. The average population in $v'=1$ for the propellant flame varied from 60-98% of the $v'=0$ population (Table 1). Nonequilibrium vibrational state populations in the OH $A_2\Sigma^+$ state in combustion environments have previously been detected in atmospheric pressure laboratory flames using emission spectroscopy.[16] In the present case, chemical processes in the propellant flame are found to also produce highly nonequilibrium populations in $v'=1$, and these populations are maintained at a high level despite the high collisional rate at these high pressures. Unfortunately, there is a large effect due to self-absorption on the apparent N_1/N_0 population ratio, which makes quantitative comparison of the results for different pressures unreliable. These self-absorption effects are discussed in more detail in the next section.

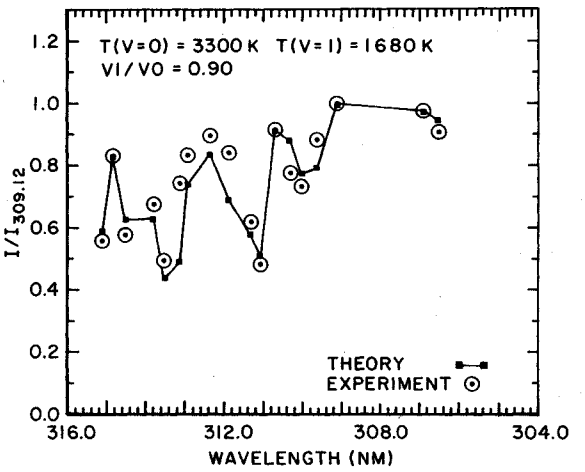

Fig. 11 Best-fit results for position = 0 μm, pressure = 3.6 MPa.

V. Self-Absorption Effects

The degree of self-absorption in individual OH emission lines depends on the line's intensity and the population in the absorbing level of the ground electronic state. Consequently, the relative intensities of the rotational-vibrational lines can change as the emitted radiation passes through the flame. The resulting spectra recorded by the detector system can thus be significantly altered due to these effects, with consequent calculated rotational temperature and vibrational distribution which may not reflect the true conditions.

To investigate the effects of self-absorption on the results shown in the previous section, a computer model has been devised and used to simulate the self-absorption of OH chemiluminescence in a high pressure flame. Briefly, the model divides the flame into small cells in which the the physical parameters are assumed constant. In each cell, the total emission intensity of each rotational-vibrational line is calculated assuming a rotational Boltzmann distribution at a given temperature and a given vibrational ratio (N_1/N_0). The emission from each cell is then followed as it passes through the remainder of the flame, with each individual spectral line absorbed in each cell by an amount determined by the rotational-vibrational population of ground electronic state OH in that cell. Spatial gradients of OH number density and rotational temperature can be specified.

Once the intensities of the rotational-vibrational lines are determined at the flame boundary, a synthetic spectrum is calculated by convoluting these intensities with a spectrometer slit function identical to that used in the analysis of the experimental spectra. In this way, a spectrum is produced which simulates what would be expected experimentally under the same flame conditions. This spectrum is then treated like the experimental spectra by taking the intensities of the same 18 peaks and finding the best fit rotational temperatures and vibrational population ratios. The desire, of course, is to ascertain whether self-absorption effects could account for some of the features of the experimental data, such as the increased deviation of particular peaks with increasing pressure. Since the actual OH ground state conditions are unknown in the propellant flame, and because the spatial gradients of OH

Table 5 Comparison of peak deviations

Pressure, MPa	Self-absorption T_R, K	Self-absorption R_1 bandhead deviation, %	Self-absorption 10th peak deviation, %	Experimental (at surface) R_1 bandhead deviation, %	Experimental (at surface) 10th peak deviation, %
0.2	2000	2.9	2.0	6.8	10.9
0.8	2000	6.8	3.1	6.2	27.0
1.8	2000	12.6	3.1	3.2	24.8
3.5	2000	20.0	2.7	2.2	23.0
7.0	2000	28.7	2.1	5.0	35.2
Peak (3.5)	2000	19.7	2.6		
Valley (3.5)	2000	19.7	2.6		
3.5	Peak (2000)	15.3	5.4		
3.5	Valley (2000)	19.0	2.3		

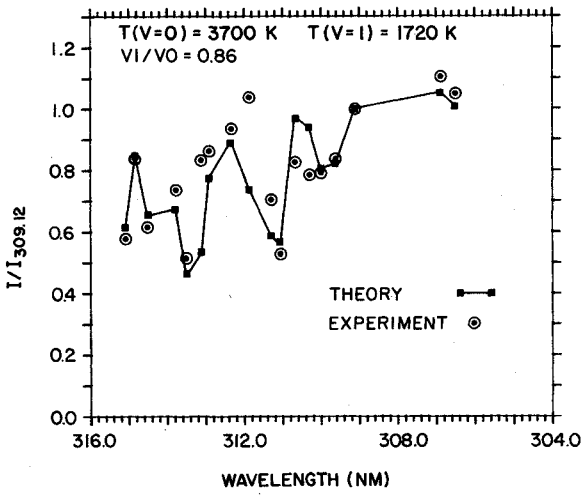

Fig. 12 Best-fit results for position = 0 μm, pressure = 7.0 MPa.

density and temperature are unknown, it is impossible to correct the experimental data for self-absorption effects. The best we can hope for is some indication of the magnitude of these effects under various conditions so as to place a bounds on the accuracy of the experimental results.

For a rotational temperature of 2000 K, a vibrational ratio (N_1/N_0) of 0.25, an OH mole fraction of 0.003, and a population in the ground electronic state of OH ten times that in the excited electronic state, the self-absorbed emission spectra for a 5-mm-diam flame (divided into 500 computational cells) were determined for pressures matching the five experimental conditions (0.2, 0.8, 1.8, 3.5, and 7.0 MPa). The best fit rotational temperatures and vibrational ratios are given in Table 3. Significant absorption effects are seen for pressures of 0.8 MPa and above, with the magnitude of the effect increasing with rising pressure (OH concentration). The best fit rotational temperature for $v'=0$ and the best fit vibrational population ratio both increase with pressure, similar to the effects seen in the experimental data. Spatial gradients of OH population and rotational temperature do not seem to have a significant effect on the results, as illustrated in Table 4 where the results for four gradient conditions are compared to the results for a flat distribution of population and rotational temperature. (for more details see Ref. 17).

The importance of possible nonequilibrium rotational distributions (in either the upper emitting or lower absorbing electronic states) is apparent when the detailed fit of the calculated self-absorbed spectra is examined and compared to the experimental results. As pressure is increased, the calculated spectra show an increasing divergence to higher intensities of the first two peaks (R_1,R_2 bandheads) from the best fit results (Table 5). In addition, the tenth peak does not diverge from the best fit significantly at any pressure. These two characteristics are diametrically counter to the results seen in the experiment, where the first two peaks always fall very close to the best fit points, and the tenth peak lies further from the best fit spectral peak as pressure is increased. Spatial gradients of OH population and rotational temperature do not affect these trends (Table 5). It is concluded from these results that self-absorption by OH ground electronic state molecules in rotational state Boltzmann equilibrium distributions cannot account for spectral features seen experimentally. Consequently, there must exist some nonequilibrium rotational population in the upper electronic state of OH due to processes involving the chemical production of excited state OH, and/or rotational nonequilibrium exists in the ground absorbing state of OH. This nonequilibrium would (of necessity) not be smooth, but it would involve the selective increase of particular rotational level populations from an equilibrium distribution in a skewed fashion. Considering the lifetime of the ground electronic state OH (long) compared to that of the excited state OH (short), the most likely conclusion is that the excited state is in nonequilibrium. Collisional redistribution of chemically produced ground electronic state OH should maintain a smooth distribution (whether in equilibrium or not) in the rotational levels.

There is no doubt that the experimental vibrational distributions are influenced by self-absorption. Comparison of the self-absorption calculation results to the experimental results shows a much larger range of calculated best-fit vibrational ratios over the pressures investigated for the self-absorption calculation than was seen experimentally. Again, the exact degree of self-absorption effects on the vibrational ratio cannot be stated with any degree of assurance, but it can be concluded that the experimental results for pressures of 0.8 MPa and above are suspect.

In summary, consideration of self-absorption effects raises some doubts about the validity of the trend toward higher T_R ($v'=0$) values with increasing pressure, as well as the accuracy of the vibrational results for pressures of 0.8 MPa and above. A detailed look at the effects of self-absorption reveals that self-absorption effects cannot account for all of the features of the experimental spectra; therefore, nonequilibrium rotational state populations in the upper emitting electronics state of OH may exist.

VI. Summary and Conclusions

OH emission spectra have been used to determine the rotational temperature and vibrational population distribution in the $A^2\Sigma^+$ state. The rotational population appears to deviate from a Boltzmann distribution for pressures above 0.8 MPa. The relative population in the $v'=1$ vibrational level was found to be much greater than would be predicted for an equilibrium population distribution at any reasonable flame temperature. The rotational temperature in $v'=1$ for many conditions can differ significantly from that in $v'=10$.

Quantitative comparison of results over a range of pressures at a given spatial position is mitigated by the potentially

significant effects of self-absorption on the measured spectra. Comparison of rotational temperatures at a given pressure for various positions above the propellant surface should be reliable if the chemical pathways of excited OH remain similar. This comparison shows that the chemically produced internal energy content of OH as reflected in the rotational state temperature is fairly constant over a very large range of distances, indicating that a chemical combustion environment involving short-lived radical species exists at distances far from the surface even at high pressures. This extended flame zone structure has recently been detected in our laboratory using various emission and laser scattering techniques in AP and HMX propellants,[5,7,18] and seems to be somewhat counter to previous propellant models which predict flame zones within tens of microns of the propellant surface.

Determination of both the rotational temperature and vibrational population of OH using emission spectra from high pressure propellant flames, although limited in accuracy due to the self-absorption effect, appears to be a useful diagnostic of propellant flame structure and chemistry. Identification of the specific chemical reactions, which produce the excited electronic state OH in its various rotational and vibrational levels, combined with computer modeling of the detailed relaxation of the internal energy states of OH at high pressures could lead to valuable insights into propellant combustion processes when combined with simple emission spectra measurements. In addition, comparisons of these emission measurement results with forthcoming laser-induced fluorescence measurements, which probe the internal energy levels of the ground electronic state, will be invaluable to further understanding of the complex process of combustion above the surface of burning solid propellants.

Appendix A: Background Correction Procedures

The OH emission spectra were found to lie on top of a background continuum which varied with position above the propellant surface and with chamber pressure. The cause of this background is at present undetermined. Its close association with the OH band emission makes it unlikely that a pseudo-continuum polyatomic-molecular-emission band is the cause. Although the linearity of the detector has not been verified in our laboratory, another group[19] has verified the linearity of their identical model diode array detector over a wide range of intensity. Furthermore, the effect does not appear to be the result of either a direct, pixel-specific sensitivity (removed by calibration) or a near-neighbor cross-talk process, but it suggests a long-range, intensity-sensitive cross-talk phenomenon. This type of long-range interference effects between diodes up to one hundred diode positions apart is highly unlikely, and has not been observed in other regions of the spectra. Furthermore, the effect seems to be pronounced toward the high-wavelength side, where the dropoff to zero is much more gradual (Fig. 8). Cross-talk and smoothing in the intensifier section of the detector are a possible cause, as is electronic buildup of charge on the detector. Electronic gating of the intensifier voltage did not appreciably change the spectral shape, so that charge buildup or failure to completely erase the previous charge is unlikely.

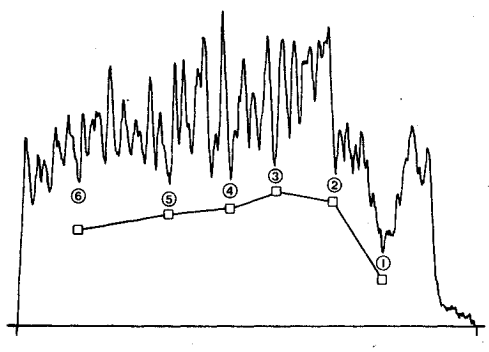

Fig. A1 Experimental spectra (position = 0 μm, pressure = 7.0 MPa) minima used to correct for background.

Irrespective of the source of this background, if the variation of background intensity with wavelength is smooth, it can be accounted for and subtracted from the experimental OH emission spectra. The method used to determine the background is as follows: 1) a rotational temperature and vibrational population distribution are guessed; 2) the synthetic spectra intensities for the 18 peaks are determined along with the intensities of 6 minima in the spectra (Fig. A1); 3) the 6 calculated minima are put on the same scale as the experimental data by assuming that maximum 3 (normalization point) will have a 10% correction due to the background; 4) six correction points are determined by subtracting each scaled calculated minimum from the corresponding experimental value; and 5) a correction for each maximum is found by a linear interpolation between the minimum correction points. The process is repeated if the correction to maximum 3 differs by more than 1% from the assumed value (10% to start). The corrected maxima are then used to find the rotational temperature and vibrational populations. If these parameters differ by more than 5% from those assumed for determination of the background correction, the whole process is repeated using these new calculated values of temperature and vibrational distribution for input to the background correction procedure. Usually only one or two repeats are necessary to converge on the corrected values. Background corrected rotational temperatures and vibrational populations typically differ from noncorrected values by less than 10% (usually much less) for most of the conditions investigated. The overall trends in the results are therefore not affected by this background correction.

Acknowledgment

This work was accomplished in part under contract to the Air Force Rocket Propulsion Laboratory (AFRPL), Air Force Systems Command, U.S. Air Force, Edwards Air Force Base, CA, Contract F04611-83-C0046; and, in part, under the Air Force Office of Scientific Research program 2308M1UZ.

References

[1]Cohen, N.S., "Review of Composite Propellant Burn Rate Modeling," *AIAA Journal,* Vol. 18, March 1980, pp. 227-291.

[2]Ben-Reuven, M. and Caveny, L. H., "Nitramine Flame Chemistry and Deflagration Interpreted in Terms of a Flame Model," *AIAA Journal,* Oct. 1981, pp. 1276-1285.

[3]Ben-Reuven, M., Caveny, L. H., Vichnevetsky, R.J., and Sommerfield, M., "Flame Zone and Sub-Surface Reaction Model for Deflagrating RDX," *Proceedings of the 16th Symposium (International) on Combustion,* The Combustion Institute, Pittsburgh, Aug. 1979, pp. 1223-1233.

[4]Miller, R. R., "Self-Extinguishment Propellant Development," Air Force Rocket Propulsion Laboratory, Edwards Air Force Base, CA, AFRPL-TR-82-096, Dec. 1982.

[5]Edwards, T., Weaver, D. P., Campbell, D. H., and Hulsizer, S., "Investigation of High Pressure Solid Propellant Combustion Using Emission Spectroscopy," *The Journal of Propulsion and Power,* Vol. 2, May-June 1986, pp. 228-234.

[6]Gaydon, A. G., *The Spectroscopy of Flames,* John Wiley and Sons, New York, 1974.

[7]Edwards, T., Weaver, D. P., Hulsizer, S., and Campbell, D. H. "Laser-Induced Fluorescence in High Pressure Solid Propellant Flames," AIAA Paper 86-0295, Jan. 1986.

[8]Goetz, F., "A High Pressure Combustion Bomb for Spectroscopic Measurements of Combustion Processes," Air Force Rocket Propulsion Laboratory, Edwards Air Force Base, CA, AFRPL-TR-80-79, Feb. 1981.

[9]Edwards, T., Weaver, D. P., Adams, R., Hulsizer, S., and Campbell, D. H. "A High Pressure Combustor for the Study of Solid Propellant Combustion Chemistry," *Journal of Scientific Instruments,* Vol. 56, Nov. 1985, pp. 2131-2137.

[10]Broida, H. P., "Rotational Temperature of OH in Methane-Air Flames," *The Journal of Chemical Physics,* Vol. 19, Nov. 1951, pp. 1383-1390.

[11]Broida, H. P. and Kostkowski, H. J., "Experimental Proof for the Existence of Nonthermal Rotational Distributions of OH ($^2\Sigma^+$) in Flames," *The Journal of Chemical Physics,* Vol. 25, Oct. 1956, pp. 676-690.

[12]Dieke, G. H. and Crosswhite, H. M., "The Ultraviolet Bands of OH," *Journal of Quantitative Spectroscopy and Radiation Transfer,* Vol. 2, 1962, pp. 97-199.

[13]Coxon, J. A., "Optimum Molecular Constants and Term Values for the $X^2\Pi(\leq 5)$ and $A^2\Sigma^+$ ($v \leq 3$) States of OH," *Canadian Journal of Physics,* Vol. 58, 1980, pp. 933-949.

[14]Chidsey, I. L. and Crosley D. R., "Calculated Rotational Transition Probabilities for the A-X System of OH," *Journal of Quantitative Spectroscopy and Radiation Transfer,* Vol. 23, 1980, pp. 187-199.

[15]Vaidya, D. B., Horvath, J. J., and Green, A. E. S., " Remote Temperature Measurements in Gas and Gas-Coal Flames Using the OH (0,0) Middle-UV Band," *Applied Optics,* Vol. 21, Sept. 1982, pp. 3357-3362.

[16]Shuler, K. E., "Kinetics of OH Radicals from Flame Emission Spectra. I. Vibrational Transition Probabilities, Intensities, and Equilibrium in the $^2\Sigma^+\Pi$ Transition," *The Journal of Chemical Physics,* Vol. 18, Sept. 1950, pp. 1221-1226.

[17]Campbell, D. H., "Self-Absorption Effects in Emission and Laser-Induced Fluroescence Diagnostics," Western States/Combustion Institute, Davis, CA, Paper 85-14, 1985.

[18]Hulsizer, S., Campbell, D. H., and Edwards, T., "2-D Visualization of High-Pressure Solid Propellant Combustion," Central States and Western States Section/The Combustion Institute, San Antonio, TX, Paper 85-5-6a, 1985.

[19]Antcliff, R. R., Hillard, M. E., and Jarrett, Jr., O., "Intensified Silicon Photodiode Array Detector Linearity: Application to Coherent Anti-Stokes Raman Spectroscopy," *Applied Optics,* Vol. 23, July 1984, pp. 2369-2374.